



PERGAMON

Deep-Sea Research II 48 (2001) 1285–1301

DEEP-SEA RESEARCH
PART II

www.elsevier.com/locate/dsr2

An annual cycle of phytoplankton biomass in the Arabian Sea, 1994–1995, as determined by moored optical sensors

C.S. Kinkade^{a,*}, J. Marra^b, T.D. Dickey^c, R. Weller^d

^aCenter for Hydro-Optics and Remote Sensing, San Diego State University, San Diego, CA 92120, USA

^bLamont-Doherty Earth Observatory of Columbia University, Palisades, NY 10960, USA

^cOcean Physics Laboratory, UCSB, Santa Barbara, CA 93106, USA

^dWoods Hole Oceanographic Institution, Woods Hole, MA 02543, USA

Received 1 September 1998; received in revised form 16 August 2000; accepted 20 August 2000

Abstract

A surface-to-bottom mooring in the central Arabian Sea (15.5°N, 61.5°E) deployed from October 1994 to October 1995, included fluorometers, PAR irradiance sensors, Lu_{683} sensors, and a spectral radiometer. An annual cycle of phytoplankton biomass was determined by transforming signals from the optical sensors into chlorophyll *a* (chl *a*). Half-yearly phytoplankton blooms with water-column stratification were observed near the end of each monsoon, as well as biomass increases in response to mesoscale flow features. During the Northeast Monsoon, the integrate water-column chl *a* rose from 15 to 25 mg m⁻², while during the Southwest Monsoon, chl *a* increased from 15 to a maximum > 40 mg m⁻². We present an empirical relationship between the ratio of downwelling E_d443/E_d550 (blue to green wavelength ratio) and integral euphotic zone chl *a* determined by moored fluorometers ($r^2 = 0.73$). There is a more significant relationship between E_d443/E_d550 measured at one depth in the water column (65 m) and the average vertical attenuation coefficient for PAR (K_{PAR}) between 0 and 65 m ($r^2 = 0.845$). Because biofouling was a significant problem at times, data return from any one sensor was incomplete. However, optical sensor/data intercomparison helped fill gaps while permitting investigation of the temporal variability in observed phytoplankton biomass. © 2001 Elsevier Science Ltd. All rights reserved.

Nomenclature

PAR photosynthetically available radiation, $\mu\text{mol photons m}^{-2} \text{s}^{-1}$ 400–700 nm
 E_0 Scalar irradiance, $\mu\text{mol photons m}^{-2} \text{s}^{-1}$

* Corresponding author. Fax: +1-619-594-8670.
E-mail address: csk@chors.sdsu.edu (C.S. Kinkade).

K_{PAR}	downward attenuation coefficient for PAR, calculated from 0 to 65 m
Z_e	Euphotic zone depth, m
Chl_{FLU}	[chlorophyll <i>a</i>] determined by moored fluorometers, mg m^{-3}
Chl_{EXT}	[chlorophyll <i>a</i>] determined by extracted shipboard bottle samples, mg m^{-3}
Chl_{683}	[chlorophyll <i>a</i>] determined by Lu_{683} sensor, mg m^{-3}
C_K	Areal euphotic zone chlorophyll <i>a</i> determined by K_{PAR} and Morel (1980), mg m^{-2}
C_F	Areal euphotic zone chlorophyll <i>a</i> determined by integrating interpolated fluorescence profiles, mg m^{-2}
C_{EXT}	Areal euphotic zone chlorophyll <i>a</i> determined by integrating extracted shipboard samples, mg m^{-2}
E_{d443}/E_{d550}	ratio of downwelling radiances at 443–550 nm

1. Introduction

Knowing the presence, absence and timing of elevated phytoplankton biomass is critical for planning studies of primary productivity, secondary biomass and productivity, and the seasonal cycle of particulate export to the deep ocean. The Arabian Sea undergoes extremes in atmospheric forcing that lead to the largest seasonal variability in surface currents, temperatures and nutrient injection observed in any ocean basin (Smith et al., 1991). Semi-annual monsoons over the Arabian Sea drive reversing basin-scale circulation patterns, unique in the world's oceans. The resulting changes in surface pressure fields and baroclinic adjustments change mixing dynamics and the nutrient supply to the euphotic zone. This forces regular oscillations in primary productivity and biomass, without relatively large changes in surface radiation or seawater temperatures, making the Arabian Sea a natural laboratory to study relationships between oceanic physical and biological processes. The extreme atmospheric forcing during the Southwest Monsoon, however, has made it logistically difficult for shipboard sampling; clouds and increased atmospheric constituents have hindered satellite remote sensing of Arabian Sea ocean color during the Southwest Monsoon. Although it is well known that there are strong seasonal changes in the Arabian Sea phytoplankton biomass, data gaps and inconsistencies have blurred the timing, magnitude and duration of the blooms (Banse, 1987).

As part of the ONR-sponsored Forced Upper Ocean Dynamics Program, which ran concurrently with the US Joint Global Ocean Flux Study (US JGOFS) Arabian Sea Expedition, five hydrographic and atmospheric moorings were deployed in the central Arabian Sea (15.5°N, 61.5°E) for two six-month deployments from October 15, 1994 to October 20, 1995 (Rudnick et al., 1997; Dickey et al., 1998; Weller et al., 1998). Multi-variable moored systems (MVMS) were deployed at 10, 35, 65 and 80 m' depth on the central surface mooring (see Sigurdson et al., 1995, 1996; Ho et al., 1996a,b; Dickey et al., 1998 for details including discussion of sensor calibration). The MVMS package included sensors to measure photosynthetically available radiation (PAR), fluorescence, natural fluorescence, beam transmission at 660 nm, dissolved oxygen, orthogonal horizontal currents, temperature and conductivity. In addition, a 32-wavelength spectral radiometer was moored at 65 m for the second half of the deployment (April 1994–October 1995). Although sensors on a mooring cannot resolve any spatial variability, the high sampling frequency of moored optical

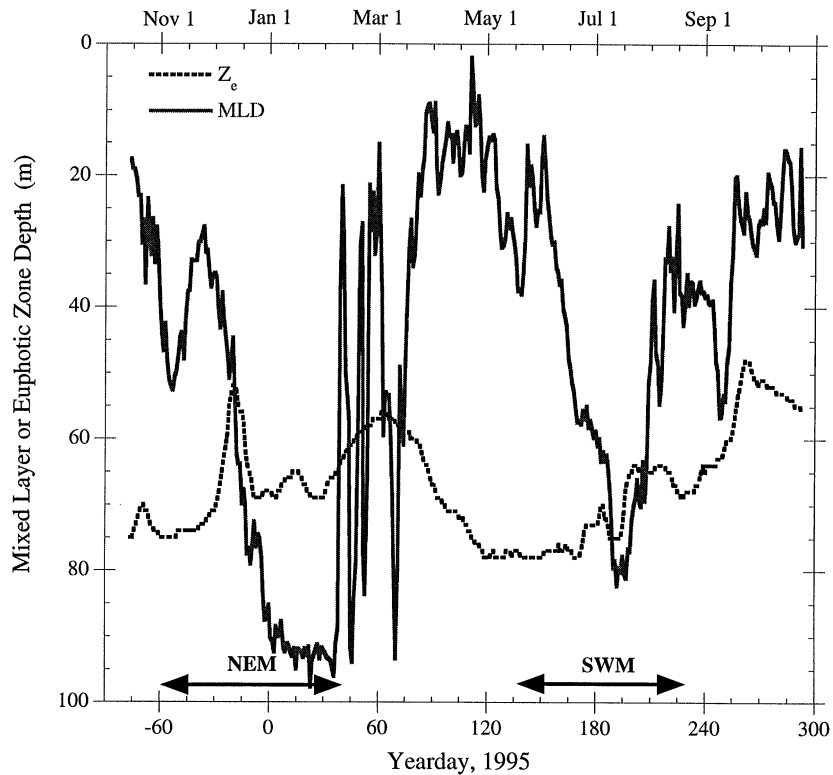


Fig. 1. Time series of mixed layer (solid line) and euphotic zone (dashed line) depths at the mooring, with times of the Northeast (NEM) and Southwest (SWM) Monsoon seasons shown.

instruments provide an excellent platform for investigating the annual and within-season cycle of phytoplankton biomass.

Here we present data from moored fluorometers, irradiance sensors and radiometers, to investigate the bio-optical response to the strong physical forcing in the central Arabian Sea. Although some fluorometric chlorophyll *a* (chl *a*) data have been presented in Dickey et al. (1998) (their Fig. 7, bottom) and as an input into the productivity model of Marra et al., 1998 (Fig. 1a), here we investigate the variability and evaluate the uncertainty in the biomass record, incorporating measurements from other optical sensors. By using analytical and empirical relationships between apparent optical properties, bio-optics and autotrophic pigments, the data from the optical sensors can be used to model the annual cycle of chl *a* biomass in the central Arabian Sea. By comparing individual sensor estimations with each other and with extracted chl *a* samples, the optical data from the mooring also can be used to help fill in data gaps due to biofouling of instruments (Ho et al., 1996a,b), add confidence to observed values of chl *a*, and investigate the observed variability in pigment biomass (Smith et al., 1991; Abbott et al., 1995), with the goal being a set of internally consistent relationships between the optical sensors.

2. Methods

2.1. Extracted chl *a* and fluorometers

Chl *a* values were obtained according to JGOFS (1996) protocol; bottle samples taken from the shipboard rosette from casts near the mooring were extracted for 24 h with 90% acetone and analyzed on a Turner Designs fluorometer. Stimulated-light fluorometers (Sea-Tech, Corvallis, OR) were moored at 10, 35, 65 and 80 m in the water column. Fluorometers are directly calibrated to chl *a*; and chl *a* concentrations derived from the fluorescence signal, Chl_{FLU} , are reported in units of mg m^{-3} . Although the fluorometers were calibrated in the laboratory prior to deployment, moored fluorescence values are subject to changes in species composition between the laboratory and field, and instrument drift caused by biofouling. In addition, there may be depth variations in the fluorescence / chl *a* ratio in the Arabian Sea (Kinkade et al., 1999) that will cause variation in calibrations (Marra and Langdon, 1993). In an attempt to minimize these errors, the extracted chl *a* values were regressed against the voltage of a profiling fluorometer on the shipboard CTD package for each depth where a fluorometer was moored (for details see Ho et al., 1996a, b). The relationship was used to ‘recalibrate’ the moored fluorometers during the field deployments as well as to evaluate instrument biofouling. All moored fluorometer data presented are daily averages of 7.5 min data, plotted at local noon.

2.2. Irradiance sensors

Although the inherent and apparent optical properties of the water column are functions of wavelength, information on the whole photosynthetic waveband is of value as a broad indication of availability of light for photosynthesis. The photosynthetically available radiation (PAR) sensors (Biospherical Instruments; San Diego, CA) moored on the array measured the scalar irradiance integrated from wavelengths of 400–700 nm, $E_{0(\text{PAR})}$. Irradiance just above the surface (E_{0+}) was calculated from an Eppley PSP pyranometer using the relationship $E_{0+(\text{PAR})} = \text{PSP} * 0.54$ (Smith and Baker, 1986). Since light decays approximately exponentially in the water column, the scalar irradiance at depth z , $E_0(z)$, is calculated by the Beer–Lambert relation:

$$E_0(z) = E_0(0^-)e^{-K \cdot z}$$

and

$$K = -\frac{d \ln E_d}{dz},$$

where K_{PAR} is the diffuse vertical attenuation coefficient for PAR. Assuming that K_{PAR} is constant with depth, Z_e is given by

$$K_{\text{PAR}} Z_e = -\ln(0.01)$$

or

$$Z_e = \frac{4.605}{K_{\text{PAR}}}$$

To convert changes in K_{PAR} to changes in autotrophic biomass, we used an empirical relationship from the statistical analysis of Morel (1980) between K_{PAR} and C_K (C_{tot} in Morel's notation). The integrated euphotic zone chl a (in units mg m^{-2}) is

$$C_K = 4910 \left(\frac{4.605}{K_{\text{PAR}}} \right)^{-1.34}.$$

2.3. Spectral Radiometer

A spectral radiometer (SR) built at the Lamont-Doherty Earth Observatory was moored at a depth of 65 m from April 22 to October 20, 1995. Technical details of SR, including materials and schematics, can be found in Maccio and Marra (1998). Briefly, the instrument consists of a compact pressure case with an Acrylite optical diffuser that was more resistant to biofouling than windows on other optical instruments deployed simultaneously. The unit uses a linear interference filter to separate the downwelling irradiance into 32 wavelengths, and a photodiode array monitors the signals at each wavelength. The data are recorded onto a Tattletale model 2B logger (Onset Instruments; Pocasset, MA). Since the SR was moored well below the depth to which red light normally penetrates, the photodiode array was adjusted to record wavelengths from 400 to 600 nm, 17 times daily (more frequently around local noon, and several times at night for dark values and clock calibration). Pre- and post-deployment calibrations were done in the laboratory, and a shipboard post-deployment comparison with a Biospherical Instruments (San Diego, CA) MER-2040 is presented in Maccio and Marra (1998). The E_d443/E_d550 ratios presented here have been corrected for possible changes in incident surface irradiance by normalization to surface PAR.

2.4. Lu_{683} sensors

Photosynthesizing algal cells re-emit about 1% of light absorbed as fluorescence (Kirk, 1994). This fluorescence, which is stimulated only by ambient light' is called solar-stimulated or natural fluorescence. Using passive fluorometers that have a response centered around 683 nm (the emission peak for chlorophyll a), measurements of the phytoplankton concentration can be made in situ without perturbing the cells. Kiefer et al. (1989) derived the mathematical equations for measuring natural fluorescence, F_f of chl a , defined as the total flux of light emitted by the chl a in a suspension of phytoplankton of unit volume under ambient light. In practice, the natural fluorometer measures Lu_{683} , the spectrally integrated radiance of a chlorophyll-like source over the viewing angle of the detector. The flux of natural fluorescence is calculated by

$$F_f = 4\pi 27(K_d + a_{683})\text{Lu}_{683},$$

where the term a_{683} is the total absorption coefficient of the water plus constituents (detritus, chlorophyll and yellow substance), which accounts for the decay of the sensed signal as a function of distance from the sensor. The term 4π is a conversion factor (in steradians) to change the radiance into a volume emission, and the factor of 27 accounts for the fluorescence bandwidth centered around 683 nm. Although Lu_{683} includes contributions from backscattered sunlight, Raman scattering, and bioluminescence, only backscattered light is significant at these wavelengths (Sugihara et al., 1984). At a depth of 65 m, it can be neglected because the signal from chl a is much

greater than the signal from backscattering (Chamberlin et al., 1990). Kiefer et al. (1989) and Chamberlin et al. (1990) showed that the concentration of chl *a* (mg m^{-3}), Chl_{683} , can be calculated from

$$\text{Chl}_{683}(z) = \frac{F_f}{a_c(\text{PAR})\phi_f E_{\text{PAR}}(z)},$$

where $E_{\text{PAR}}(z)$ is the irradiance that is PAR at depth z , $a_c(\text{PAR})$ is the chl *a* specific absorption coefficient of the phytoplankton and ϕ_f is the quantum yield of fluorescence. The assumption must be made that these last two coefficients are constant, which is discussed below. We use values for $a_c(\text{PAR})$ and ϕ_f published by Kishino et al. (1984b), 0.04 and 0.045, respectively. We found, as did Abbott et al. (1995), that using coefficients published by Chamberlin et al. (1990), ($a_c(\text{PAR}) = 0.016$ and $\phi_f = 0.028$) yielded chl *a* values consistently higher than those obtained by fluorometers and extracted bottle samples by up to a factor of five.

2.5. Other instruments

Transmissometers were deployed on the mooring; however, the larger optical windows on the transmissometers made them more susceptible to biofouling. More importantly, the conversion of transmissometer data to chl *a* requires assumption of a beam-c:POC ratio (which varies seasonally; Gundersen et al., 1998) and a carbon:chl *a* ratio (which will vary with cellular physiological state and irradiance history). These variations make transmissometer-based estimations of chl *a* less robust over seasonal or annual time scales; thus, no transmissometer data are presented here.

Although the mooring was deployed during the 1994 Fall Intermonsoon, all data are referenced to 1995 yeardays; seasonal definitions are Fall Intermonsoon (mooring deployment 14 October, 1994 to 31 October, 1994; yeardays – 77 to – 61); Northeast Monsoon, (1 November, 1994 to 15 February, 1995; yeardays – 60 to 46); Spring Intermonsoon (16 February, 1995 to 31 May, 1995; yeardays 47 to 151); and Southwest Monsoon (1 June, 1995 to 15 September, 1995; yeardays 152 to 258).

The mooring was instrumented with 29 temperature sensors in the upper 175 m (Weller et al., 1998). Mixed-layer depth (MLD) was calculated as a 0.1°C temperature difference from the surface. Shipboard data come from samples obtained during mooring cruises (yeardays – 78, – 76, 44, 108, and 109) or from US JGOFS Arabian Sea station *S7* when the *R/V Thompson* was nearest the mooring (cruises TN043, yearday 23; TN045, yearday 89; TN049, yearday 217; TN050, yearday 248; and TN 053, yearday 318; see Smith et al., 1998 for cruise schedules). These data can range up to 100 km away from the mooring anchor position. The shipboard K_{PAR} was calculated from sensors on a drifting array (Barber et al., 1997), minimizing ship shadowing of the upper PAR sensors. All shipboard bottle data and PAR profiles can be found on the US JGOFS website, <http://usjgofswww.who.edu>.

3. Results

Fig. 1 shows the record of MLD and Z_e . There is a semi-annual cycle of deepening and shoaling of the mixed layer. During the 1994 winter NE Monsoon, the MLD deepens from 20 to about

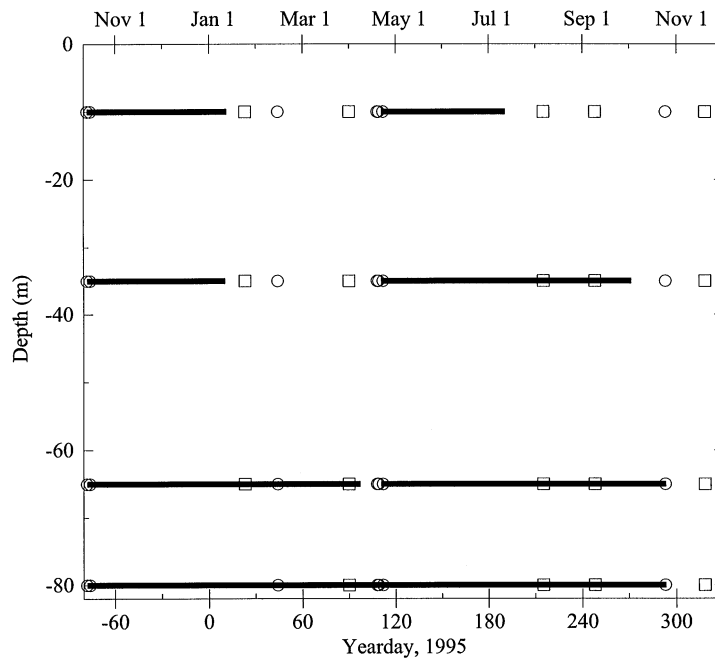


Fig. 2. Time-line of fluorometer data return at 10, 35, 65 and 80 m depth for the two 6-month mooring deployments. Also plotted are times and depths of shipboard extracted chl *a* samples at the mooring (open circles) and at US JGOFS Arabian Sea station S7 (open squares). These data were used as input for the gridding routine used to create Fig. 3.

100 m, but the effects of an advective event shoaling the mixed layer in November can be seen. As the winds slack with the Spring Intermonsoon period, the sign of the net heat flux changes (Fischer, 1997; Weller et al., 1998), and the MLD shoals as the upper water column restratifies. In June, when the SW Monsoon winds pick up, the mixed layer deepens again to about 75 m. Shortly after the spin-up of the Southwest Monsoon, the average MLD deepens from 20 to 80 m by July 1, largely due to wind driven overturn (Rudnick et al., 1997; Weller et al., 1998). Another advective event can be discerned from the end of July into August, 1995 as the MLD shoals slowly despite strong winds.

The timeline of data return from the 10, 35, 65 and 80 m fluorometers is plotted as horizontal black lines in Fig. 2. Also, plotted are the times and depths when shipboard extracted chl *a* samples are available. The open circles are from water samples taken at the mooring site (yeardays - 78, - 76, 44, 108 and 109) and open squares are chl *a* samples from the US JGOFS station S7 (yeardays 23, 89, 112, 215, 248, and 318). These data were interpolated both in depth and time using routines of the Generic Mapping Tools (Wessel and Smith, 1991) to estimate the seasonal cycle of phytoplankton biomass. Fig. 3 is a probable representation of a time-depth slice of the fluorometer-based pigment biomass for the year long mooring deployments. The dashed boxes enclose the times and depths when only shipboard data (see Fig. 2) were used in the gridding routine. There is a clear semiannual response in fluorometer pigment biomass, with high concentrations at the end of each monsoon season. In addition, there are elevated, near-surface pigment

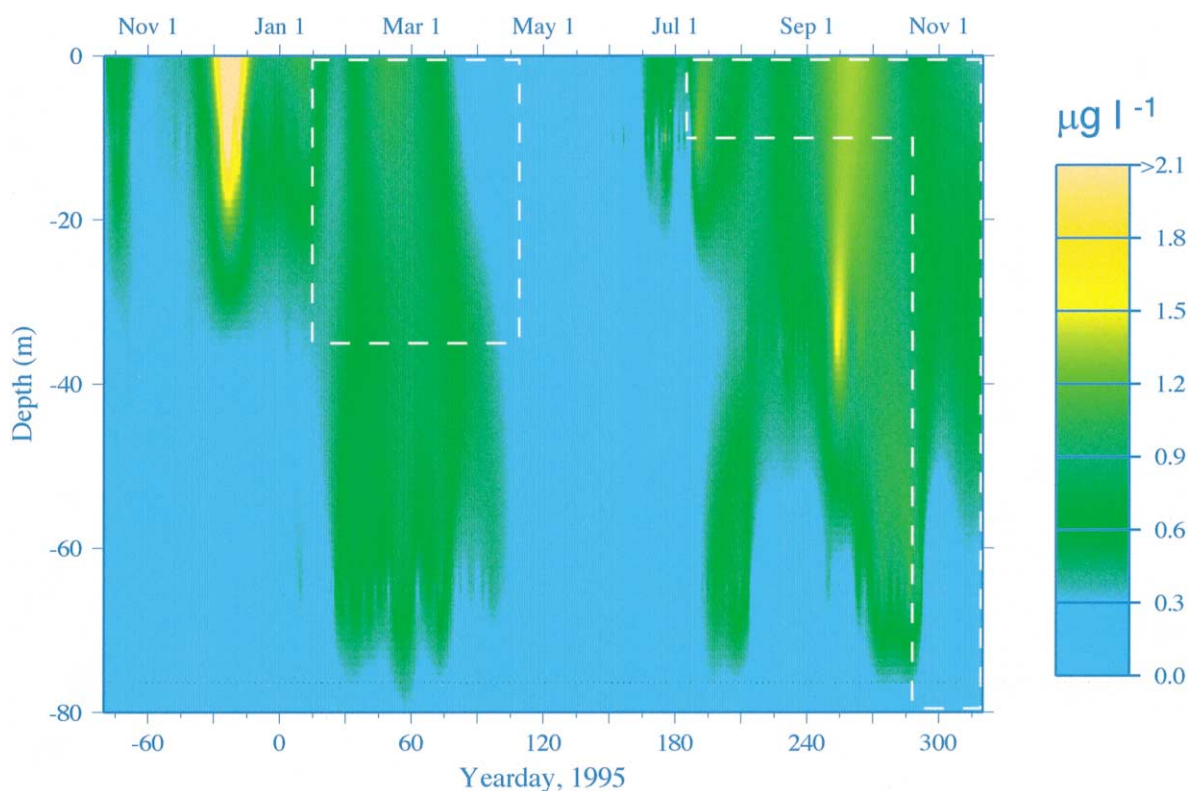


Fig. 3. Time-depth section of chl *a* concentration from fluorometers, with concentration color scale at right. White dashed boxes enclose times and depths where moored fluorometers were subject to fouling, and shipboard extracted chlorophyll *a* values have been used in the gridding and contouring routines.

concentrations associated with geostrophic flow features that passed through the array (Dickey et al., 1998). The first of these, a cold-core mesoscale feature was observed in November and December 1994 (yeardays -45 to -20 ; Sigurdson, 1995). The second mesoscale feature lifted the thermocline beginning in mid-July through early September (yeardays 197–258).

Fig. 4 presents K_{PAR} transformed into integral euphotic zone chl *a*, C_K . The C_K time series is plotted over a color time-depth slice of temperature to give hydrographic reference for the changes in biomass. The data become noisy toward the end of the record because of the lower number of photons reaching the 65-m sensor with the shoaling of the euphotic zone. Also plotted, in filled circles, is the Chl_{ext} integrated over Z_e for times when the ship was near the mooring. Given spatial variability, these points agree well with the optical C_K . Higher integral phytoplankton biomass is associated with cooler temperatures in the upper 70 m and stratification of the water column during both monsoon seasons. When the mixed layer is deep, there are low values of integrated water column chl *a*. In addition to these seasonal changes, the phytoplankton biomass responds to the mesoscale cold feature from yeardays -45 to -20 , increasing to $\sim 25 \text{ mg m}^{-2}$. With the water column stratification after July 1, the mixed layer shoals, and C_K rises nearly four-fold.

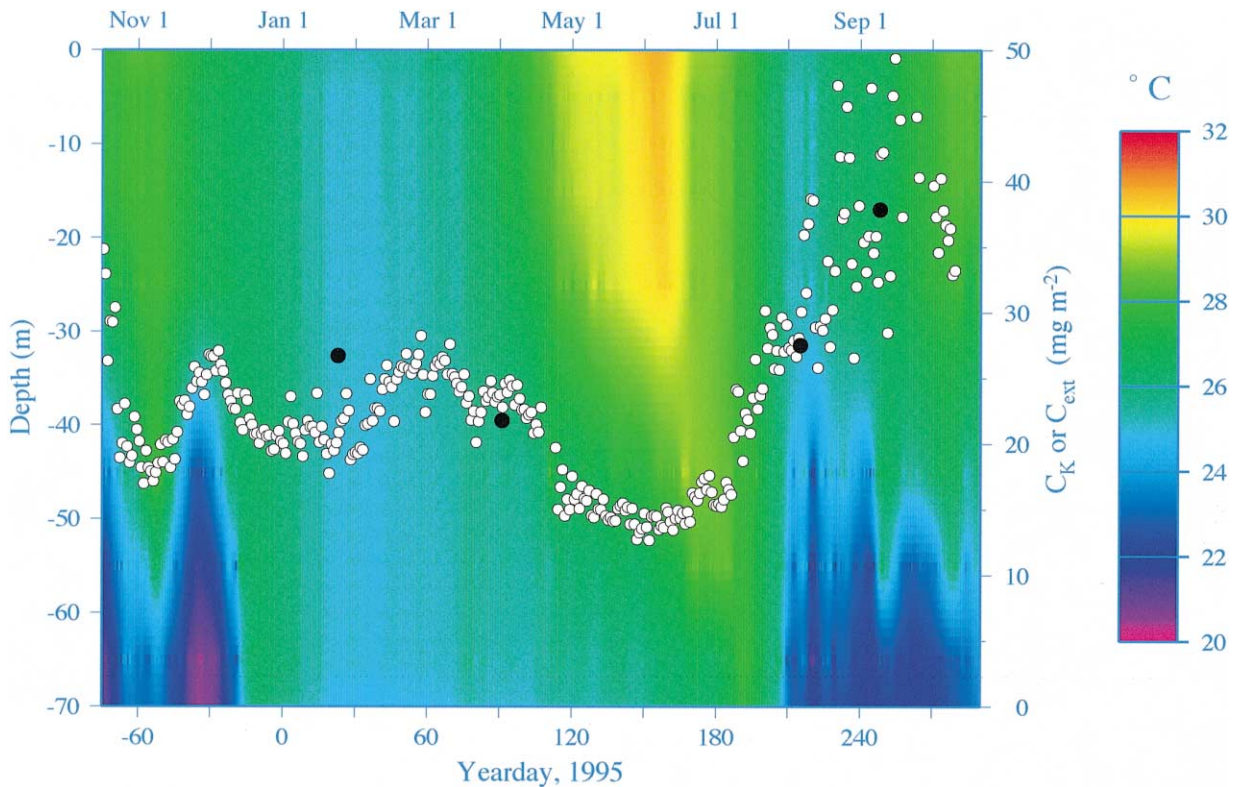


Fig. 4. Time-depth section of water column temperature ($^{\circ}\text{C}$, in color, with scale bar at far right), with C_K biomass estimates (open circles, scale on right axis) and shipboard C_{EXT} measurements (closed circles).

To compare optical estimates of biomass integrated over the euphotic zone, the fluorometric C_F is plotted with C_K in Fig. 5. The two curves do not match well during yeardays -45 to 90 , when the fluorescence estimate of integrated, water-column pigment biomass is a factor of 2.5 higher during the mesoscale eddy passage, and 3 times higher after the Northeast Monsoon. This major difference is discussed below. The 65-m Chl_{683} estimate of pigment biomass is plotted along with the 65 m Chl_{flu} in Fig. 6. The two estimates match extremely well until about yearday 190, when water-column stratification begins during the Southwest Monsoon.

Fig. 7 shows temperature contours in the upper 75 m of the water column, the euphotic zone depth, and the irradiances at 443 nm (blue) and 550 nm (green) from May to September, 1995. A generally increasing trend can be seen in the peak irradiance at the blue wavelength 443 nm from yeardays 120–160, and then a steady decrease with the mesoscale feature and subsequent spin-up of the Southwest Monsoon. During the time this eddy passed, the euphotic zone shoaled to 65 m, and then up to 50 m with the Southwest Monsoon phytoplankton bloom. The decline in irradiance at the green wavelength 550 nm appears to start later than that at 443 nm by about 3 weeks. Fig. 8 shows E_d443/E_d550 at local noon (dashed curve), and smoothed with a 5-day moving average filter (solid curve). This blue-to-green ratio increases from May until the middle of June,

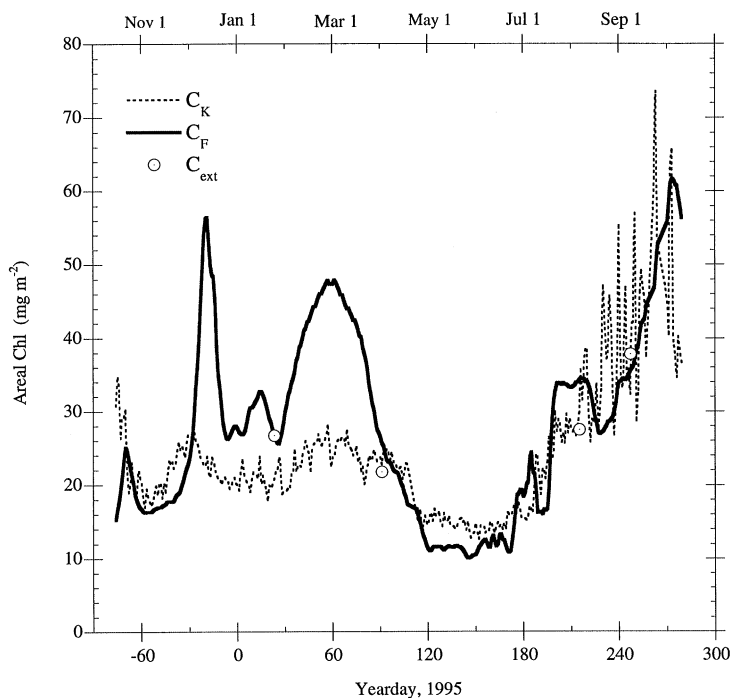


Fig. 5. Integrated water-column chlorophyll *a* biomass determined from irradiance sensors (C_K , dashed line), determined from moored fluorescence profiles (C_F , solid line), and from shipboard extracted chlorophyll profiles (C_{EXT} , open circles).

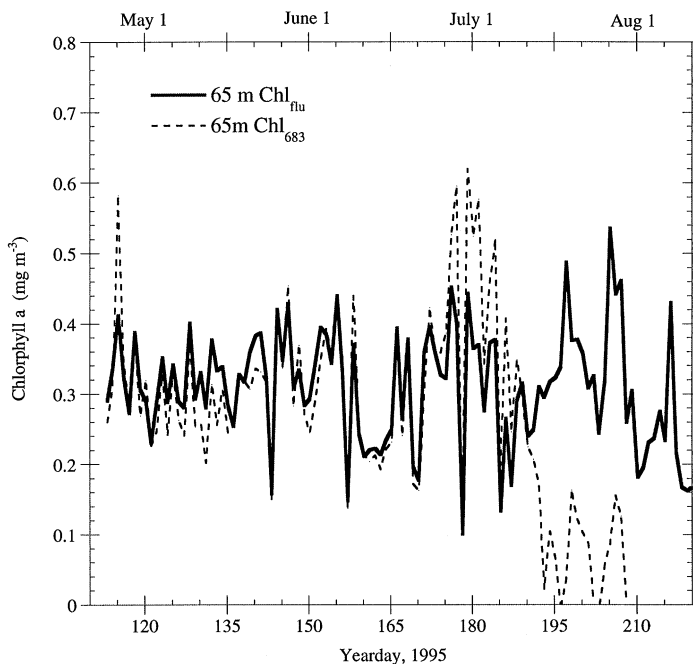


Fig. 6. Chl_{FLU} (solid line) and Chl_{683} (dashed line) at 65 m during the second 6-month mooring deployment.

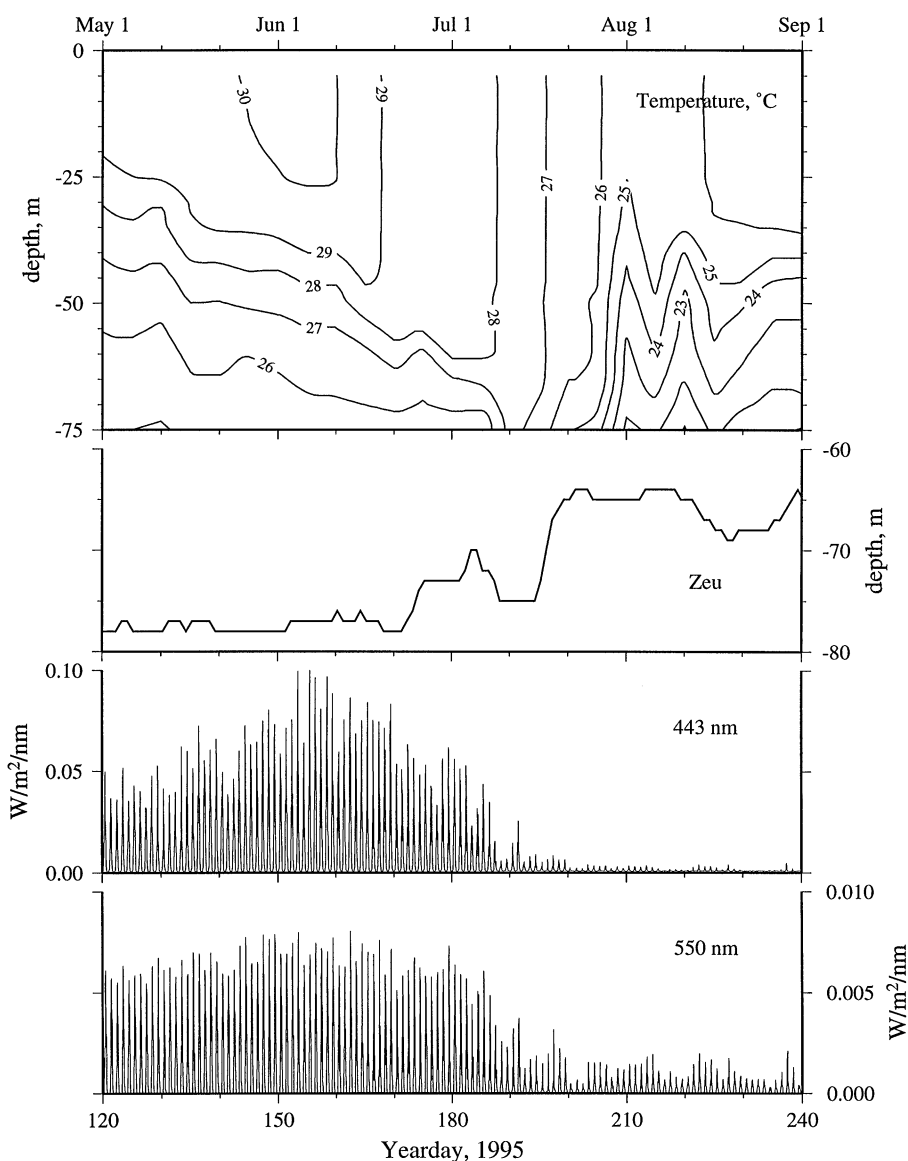


Fig. 7. From top to bottom: temperature structure of the upper 75 m of the water column ($^{\circ}\text{C}$), euphotic zone depth (m), downwelling irradiance at 443 nm, and downwelling irradiance at 550 nm, from \sim May 1 to \sim September 1, 1995.

drops with the biomass increase associated with the passing of the eddy flow-feature, then rises again before decreasing sharply with the Southwest Monsoon phytoplankton bloom in August. Using ratios of irradiances has the benefit of being less dependent on instrument orientation with respect to incident solar angle; any instrument cosine variations will be minimized by utilizing pairs of irradiances. The irradiance ratio models, like the one used here, have provided the best biomass estimates, but there is evidence that model (regression) coefficients may vary with depth (Smith

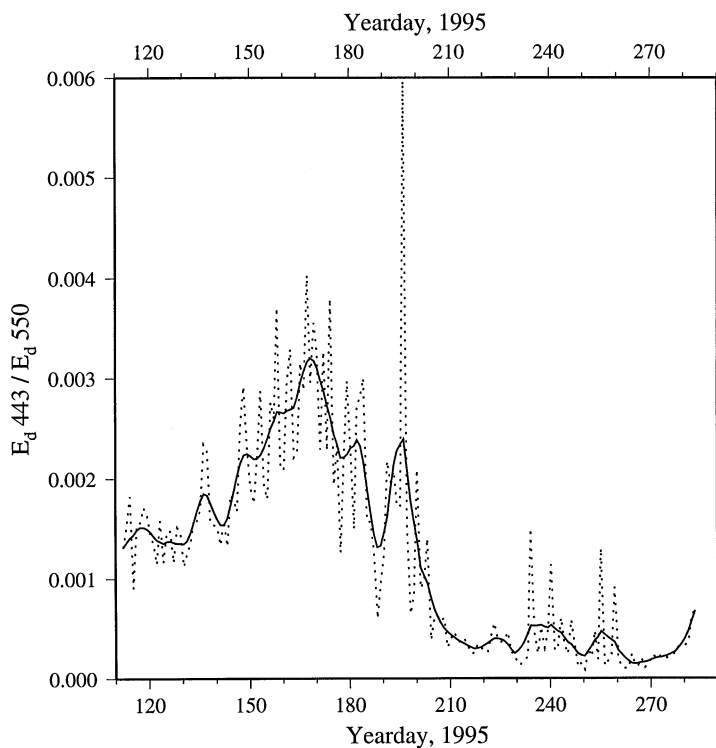


Fig. 8. The ratio of $E_d 443/E_d 550$ normalized to surface PAR (to correct for atmospheric effects). Dashed line is data from local noon, solid line has been smoothed with a 5-day moving average filter.

et al., 1991). Fig. 9 plots $E_d 443/E_d 550$ against (a) C_{FLU} , the fluorometer chl a integrated over the euphotic zone. The regression coefficient ($r^2 = 0.74$) is within the range of past empirical relationships of optical quantities in open-ocean waters using large, global data sets (Loisel and Morel, 1998). Fig. 9(b) plots average K_{PAR} from 0 to 65 m. The least-squares fit gives an $r^2 = 0.84$.

4. Discussion

The two monsoon seasons in the Arabian Sea result in two periods of mixed-layer deepening near the beginnings of each monsoon, in December and June. Intense surface cooling due to the air-sea temperature difference leads to a net heat flux out of the ocean, and convective overturning during the winter Northeast Monsoon (Fischer, 1997; Weller et al., 1998). During this period, the MLD depth reaches its yearly maximum of about 100 m. The much stronger Southwest Monsoon winds, sustained above 10 m s^{-1} throughout the Southwest Monsoon and peaking above 18 m s^{-1} (Weller et al., 1998), produced a maximum MLD of 70 m. Acoustic Doppler current profilers (ADCP) showed regions of high shear located just beneath the mixed-layer base, enhancing turbulent entrainment into the mixed-layer (Rudnick et al., 1997).

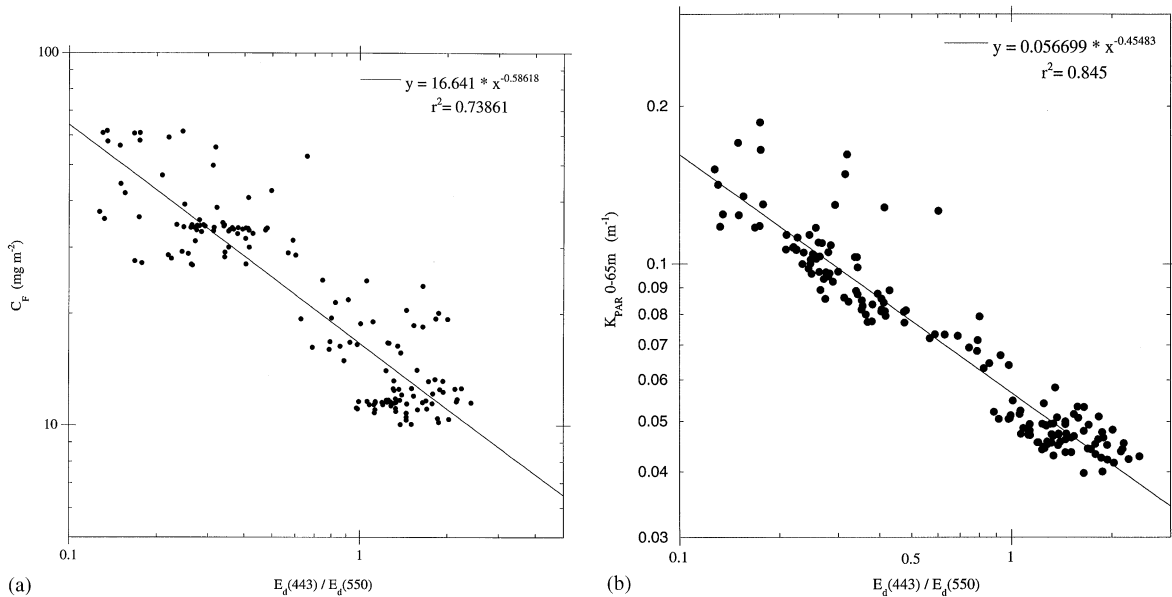


Fig. 9. (a) PAR normalized $E_d(443)/E_d(550)$ plotted against average K_{PAR} . The power law fit gives an $r^2 = 0.84$. (b) $E_d(443)/E_d(550)$, plotted against C_F (fluorometer chl *a* integrated over the euphotic zone).

The dominant physical variability of twice-yearly mixed-layer deepenings drives semi-annual phytoplankton responses. Higher integral euphotic zone phytoplankton biomass was associated with the restratification that occurred at the end of both monsoon periods. When there are cooler water temperatures in the upper 70 m associated with the mixed-layer shoalings, the euphotic zone extends into cooler, presumably more nutrient-rich water, allowing phytoplankton growth. This effect may be enhanced by later stratification, which acts to accumulate biomass. In addition, reduced zooplankton grazing pressure in August (Smith et al., 1998b) could allow increased autotrophic biomass during the Southwest Monsoon. During the strong stratification in the Spring Intermonsoon period, there were low phytoplankton biomass concentrations, probably from exhaustion of nutrients, limiting growth.

Monsoonal winds drive coastal upwelling and currents along the Omani coast, which have been observed to shed filaments and eddies of cold water far into the Arabian Sea (Brink et al., 1998). Flagg and Kim (1998) note the complete dominance of the velocity field in the Arabian Sea by eddies that had offshore correlation length scales of ~ 100 km. The dominant basic cycle of monsoonal phytoplankton growth is augmented by the phytoplankton response to the intense mesoscale activity of the Arabian Sea, which in December 1994 led to a biomass increase comparable to that during the Northeast Monsoon (Fig. 4).

The C_F and C_K curves (Fig. 5) do not track each other well during yeardays – 45 to 80 when the C_F values are higher by up to a factor of 2 just after the Northeast Monsoon and by a factor of nearly 3 during the advective event. During the period of eddy passage and the end of the

Northeast Monsoon, the MLD is greater than Z_e , or at least variable during water-column stratification (Fig. 1), and the bottom of the euphotic zone is above the 65-m PAR sensor. The C_K estimate uses an average K_{PAR} from 0 to 65 m, but when Z_e is above 65-m, one average K_{PAR} for above and below the euphotic zone will not be accurate. This would tend to make the average K_{PAR} too low, resulting in a lower estimate of integrated water-column pigment biomass. The C_F and C_K models should always be in better agreement when $Z_e > 65$ m and the phytoplankton are confined to a mixed layer more shallow than the optical sensor. Also, during high fluorescence peaks, the sparse vertical fluorescence data interpolated by the gridding routine will tend to make C_F higher than C_K , during the time period just after the Northeast Monsoon, for example. It is likely that a combination of these two processes leads to the observed divergence of the two biomass estimates. The two curves and the shipboard extracted data agree for the second half of the year.

In Fig. 6, the Chl_{683} and Chl_{FLU} estimates of phytoplankton biomass match very well until about a month after the spin-up of the Southwest Monsoon, and the mixed layer begins to shoal around yearday 195. At this time, the phytoplankton composition near the mooring shifts to a community dominated by diatoms (R. Bidigare, pers. comm.). Chl_{683} can be very consistent with the stimulated fluorescence chlorophyll concentrations, although the relationship depends completely on the chosen quantum yield of fluorescence and absorption coefficient for PAR being constant, which is not likely in natural populations. Without more information, such as inherent optical properties, we are using Chl_{683} here as an empirical model. As a result, divergences in the two curves can be diagnostic for community changes in the water column.

There are several potential sources of error in this optical sensor intercomparison. Integrating over all PAR wavelengths is an oversimplification. In reality, all inherent and apparent optical properties are functions of wavelength. Although the commonly accepted first-order proxy, chl *a* itself, it is a rough measure of phytoplankton biomass because in vivo chl *a* is subjected to variability such as photoadaptation and photoinhibition (Kirk, 1994). There is a diel variability in the chl *a* fluorescence signals (Kinkade et al., 1999), which is not seen because of daily averaging. There are some divergences in the optical biomass estimates, notably where sampling is poor because of instrument (fouling or gain) problems, or where there are changes in assumed physiological parameters of the community. Our empirical relationship between integral fluorometric chl *a* and E_d443/E_d550 is less coherent during times when the pigment biomass is greatest; at these times fewer photons reach the SR at 65 m. The relatively poor vertical resolution of 4 fluorometers moored in the upper 80 m of the water column and the gridding and contouring of sparse data will add to the errors in our biomass models. In general, however, the intercomparison has shown largely internally consistent relationships between the optical sensors in determining a yearly cycle of autotrophic biomass in the Arabian Sea.

Comparison with the 1980–1995 means produced by the Southampton Oceanography Center (Josey et al., 1996, 1997a) shows that 1994–1995 was a typical year for surface meteorology and air-sea fluxes, with values within one standard deviation of the long-term means (Weller et al., 1998). Interannual variability of biological and bio-optical data is less well known than the atmospheric variability, however.

Since upwelling is primarily driven by wind-stress curl associated with the Findlater Jet, interannual variability in the strength and position of the jet will lead to variability in upwelling. A weaker or less-defined jet has weaker cyclonic curl, leading to reduced coastal upwelling. There is

a correlation between interannual variability in the Asian monsoon system and El Niño events in the Pacific Ocean. During an El Niño event in 1987, warm sea-surface temperature anomalies during the summer Southwest Monsoon produced large-scale atmospheric circulation anomalies that weakened the Findlater Jet and the Somali Current, leading to a weaker Arabian Sea circulation (Krishnamurti et al., 1989). These conditions would tend to cause less coastal upwelling and lower phytoplankton pigment concentrations during the Southwest Monsoon. During the strong El Niño event of 1982–1983, Brock and McClain (1992) reported weak Ekman upwelling velocities, and much lower CZCS pigment concentrations in the Arabian Sea than during the previous three years. Both the Southern Oscillation Index and the NINO-3 index (both available from <http://www.rainbow.ldeo.columbia.edu>) showed weak El Niño conditions during the 1994 Northeast Monsoon, and close to zero pressure and temperature anomalies during the 1995 Southwest Monsoon. Thus, in terms of response to the monsoons, we probably sampled fairly ‘average’ biological conditions in the 1994–1995 year.

Moored spectral irradiance sensors cannot provide synoptic views on the scale of ocean basins, but they have some advantages over satellite spectral instruments. Roughly 90% of the satellite-sensed ocean signal comes from the top attenuation length of the water column (Gordon and McCluney, 1975), which is inversely proportional to K_{PAR} . Since the depth distribution of pigment biomass is controlled by physical processes that vary with location and time, satellite estimates of chl *a* have been shown to underestimate total chl *a* in the water column, because of the deep chlorophyll maximum often present in open ocean waters (e.g., Cullen, 1982). Satellite sensors cannot collect ocean color data when clouds obscure views of the ocean surface. The same processes that cause cloudiness (e.g., episodic wind events) also can give rise to changes in water column pigment biomass (upwelling of nutrients and subsequent phytoplankton production). Thus, satellite observations may not be random samples (Michaelsen et al., 1988). Measurements of in situ ocean color from submerged spectral instruments, however, can be obtained in all atmospheric conditions.

Although normally K_{PAR} (or K_{λ}) is measured from at least two depths in the water column, obtaining estimates of this apparent optical property from a single depth using downwelling irradiances (submerged remote sensing; Petzold and Austin, 1987) or from satellite using upwelling irradiances (Austin and Petzold, 1981) has been of interest. Here we have developed an empirical relationship between an average water column K_{PAR} between 0 and 65 m, and E_d443/E_d550 measured at one depth. In addition to simply fewer sensor requirements, possible applications include estimation of optical communication channel attenuation above a submerged submarine during daylight hours. Petzold and Austin (1987) have incorporated ocean water and atmospheric losses into multi-wavelength irradiance ratios toward this end.

When determining mechanistic links between physical processes (e.g., wind-stress curl) and biological response (e.g., pigment biomass increase) several authors have suggested a lag between the spin-up of the Southwest Monsoon winds and maximum autotrophic pigment concentrations (Smith et al., 1991; Yentsch and Phinney, 1992; Bartolacci and Luther, 1999). Although the mesoscale feature passing by the mooring makes it difficult to establish the start of the pigment response to the monsoonal physical forcing from our data, the spectral irradiance ratio response shows that maximum integral pigments, (and thus the lowest E_d443/E_d550) are reached around the first week in August, about 2 months after the increase in the monsoonal winds at the beginning of June (Fig. 8).

Acknowledgements

This research was supported by ONR grants N00014-94-0450 (JM), N00014-96-1-0505 (DD), and N00014-94-1-0161 (RW). This is US JGOFS contribution number 495.

References

- Abbott, M.R., Brink, K.H., Booth, C.R., Blasco, D., Swenson, M.S., Davis, C.O., Codispoti, L.A., 1995. Scales of bio-optical properties as observed from near-surface drifters. *Journal of Geophysical Research* 100, 13345–13367.
- Austin, R.W., Petzold, T.J., 1981. The determination of the diffuse attenuation coefficient of sea water using the Coastal Zone Color Scanner. In: Gower, J.R.R. (Ed.), *Oceanography from Space*. Plenum Publishing, New York, pp. 239–256.
- Banse, K., 1987. Seasonality of phytoplankton chlorophyll in the central and northern Arabian Sea. *Deep-Sea Research* 34, 713–723.
- Barber, R.T., Borden, L., Johnson, Z., Marra, J., Knudson, C., Trees, C., 1997. Ground truthing modeled k_{par} and on deck primary productivity incubations with in situ incubations. In: Ackleson, S., Frouin, R. (Eds.), *Ocean Optics XIII Proceedings of SPIE*, Vol. 2963, pp. 834–839.
- Bartolacci, D., Luther, M., 1999. Patterns of co-variability between physical and biological parameters in the Arabian Sea. *Deep-Sea Research II* 46, 1933–1964.
- Brink, K., Arnone, R., Coble, P., Flagg, C., Jones, B., Kindle, J., Lee, C., Phinney, D., Wood, M., Yentsch, C., Young, D., 1998. Monsoons boost biological productivity in Arabian Sea. *EOS* 79, 168–169.
- Brock, J.C., McClain, C.R., 1992. Interannual variability in phytoplankton blooms observed in the northwestern Arabian Sea during the southwest monsoon. *Journal of Geophysical Research* 97, 733–750.
- Chamberlin, W.S., Booth, C.R., Kiefer, D.A., Morrow, J.H., Murphy, R.C., 1990. Evidence for a simple relationship between natural fluorescence, photosynthesis, and chlorophyll in the sea. *Deep-Sea Research* 37, 951–973.
- Cullen, J.J., 1982. The deep chlorophyll maximum: comparing vertical profiles of chlorophyll *a*. *Canada Journal of Fisheries and Aquatic Science* 39, 791–803.
- Dickey, T.D., Marra, J., Sigurdson, D.E., Weller, R.A., Kinkade, C.S., Zedler, S.E., Wiggert, J.D., Langdon, C., 1998. Seasonal variability of bio-optical and physical properties in the Arabian Sea: October 1994 – 1995. *Deep-Sea Research II* 45, 2001–2026.
- Fischer, A., 1997. Arabian Sea mixed layer deepening during the monsoon: observations and dynamics. S.M. thesis, Massachusetts Institute of Technology, Boston, 130 pp.
- Flagg, C.N., Kim, H.-S., 1998. Upper Ocean Currents in the northern Arabian Sea from shipboard ADCP measurements collected during the 1994–1996 US JGOFS and ONR programs. *Deep-Sea Research II* 45, 1917–1960.
- Gordon, H.R., McCluney, W.R., 1975. Estimation of the depth of sunlight penetration in the sea for remote sensing. *Applied Optics* 19, 413–416.
- Gundersen, J.S., Gardner, W.D., Richardson, M.J., Walsh, I.D., 1998. Effects of monsoons on the temporal and spatial variations of POC and chlorophyll in the Arabian Sea. *Deep-Sea Research II* 45, 2103–2132.
- Ho, C., Kinkade, C., Langdon, C., Maccio, M., Marra, J., 1996a. The Forced Upper Ocean Dynamics experiment in the Arabian Sea. Results from the multi-variable moored sensors from deployment-1 of the WHOI mooring. LDEO technical report LDEO-96-5, Lamont Doherty Earth Observatory, Palisades, NY, 19 pp. + figs.
- Ho, C., Kinkade, C., Langdon, C., Maccio, M., Marra, J., 1996b. The Forced Upper Ocean Dynamics experiment in the Arabian Sea. Results from the multi-variable moored sensors from deployment-2 of the WHOI mooring. LDEO technical report LDEO-96-8, Lamont Doherty Earth Observatory, Palisades, NY, 19 pp. + figs.
- Josey, S.A., Kent, E.C., Oakley, D., Taylor, P.K., 1996. A new global air-sea heat and momentum flux climatology. *International WOCE Newsletter* 24, pp. 3–5.
- Kiefer, D.A., Chamberlin, W.S., Booth, C.R., 1989. Natural fluorescence of chlorophyll *a*: Relationship to photosynthesis and chlorophyll concentration in the western South Pacific gyre. *Limnology and Oceanography* 34, 868–881.
- Kinkade, C.S., Marra, J., Dickey, T., Langdon, C., Sigurdson, D.E., Weller, R., 1999. Diel bio-optical variability observed from moored sensors in the Arabian Sea. *Deep-Sea Research Part II* 46, 1813–1832.

- Kirk, J.T.O., 1994. *Light and Photosynthesis in Aquatic Ecosystems*. 2nd Edition, Cambridge University Press, New York, 256 pp.
- Kishino, M., Sugihara, S., Okami, N., 1984b. Estimation of quantum yield of chlorophyll a fluorescence from the upward irradiance spectrum in the sea. *La Mer* 22, 233–240.
- Krishnamurti, T.N., Bedi, H.S., Subramaniam, M., 1989. The summer monsoon of 1987. *Journal of Climate* 2, 321–340.
- Loisel, H., Morel, A., 1998. Light scattering and chlorophyll concentration in case 1 waters: A reexamination. *Limnology and Oceanography* 43, 847–858.
- Maccio, M., Marra, J., 1998. A low-cost, compact, moored spectral radiometer. LDEO Technical Report LDEO-98-4, Lamont Doherty Earth Observatory, Palisades, NY, 20 pp. + 12 figs.
- Marra, J., Chamberlin, W.S., Knudson, C., 1993. Proportionality between in situ carbon assimilation and bio-optical measures of primary production in the Gulf of Maine in summer. *Limnology and Oceanography* 38, 232–239.
- Michaelsen, J., Zhang, X., Smith, R.C., 1988. Variability of pigment biomass in the California Current system as determined by satellite imagery. Part II: Temporal variability. *Journal of Geophysical Research* 93, 10 883–10 896.
- Morel, A., 1980. Optical modeling of the upper ocean in relation to its biogenous matter content (case I waters). *Journal of Geophysical Research* 93, 10 749–10 768.
- Petzold, T.J., Austin, R.W., 1987. Remote sensing of atmospheric optical thickness and sea-water attenuation when submerged: wavelength selection and anticipated errors. Scripps Institution of Oceanography Technical Report No. SIO 87-18, Scripps Institution of Oceanography, La Jolla, CA, 84 pp.
- Rudnick, D., Weller, R.A., Eriksen, C., Dickey, T.D., Marra, J., Langdon, C., 1997. One-year moored observations of the Arabian Sea Monsoons. *EOS* 78, 120–121.
- Sigurdson, D.E., Dickey, T.D., Manov, D., 1995. Arabian Sea mooring data report: Deployment No. 1, October 15, 1994 – April 20, 1995. Ocean Physics Laboratory Technical Report No. OPL-2-95, University of California, Santa Barbara, CA, 163pp.
- Sigurdson, D.E., Dickey, T.D., Manov, D., 1996. Arabian Sea mooring data report: Deployment No. 2, April – October 20, 1995. Ocean Physics Laboratory Technical Report No. OPL-2-96, University of California, Santa Barbara, CA, 134pp.
- Smith, R.C., Baker, K.S., 1986. The analysis of ocean optical data II. In: *Ocean Optics VIII*, Proc. SPIE 637, 95–107.
- Smith, R.C., Waters, K.J., Baker, K.S., 1991. Optical variability and pigment biomass in the Sargasso Sea as determined using deep-sea optical mooring data. *Journal of Geophysical Research* 96, 8665–8686.
- Smith, S.L., Banse, K., Cochran, J.K., Codispoti, L.A., Ducklow, H.W., Luther, M.E., Olson, D.B., Peterson, W.T., Prell, W.L., Surgi, N., Swallow, J.C., Wishner, K., 1991. U.S. JGOFS: Arabian Sea Process Study, U.S. JGOFS Planning Report No. 13, Woods Hole Oceanographic Institution, Woods Hole, Massachusetts, 164 pp.
- Smith, S.L., Roman, M., Prusova, I., Wishner, K., Gowing, M., Codispoti, L., Barber, R.T., Marra, J., Flagg, C., 1998b. Seasonal response of mesozooplankton to monsoonal reversals in the Arabian Sea. *Deep-Sea Research Part II* 45, 2369–2404.
- Sugihara, S., Kishino, M., Okami, N., 1984. Contribution of Raman scattering to upward irradiance in the sea. *Journal of the Oceanographical Society of Japan* 40, 397–404.
- Weller, R.A., Baumgartner, M.F., Josey, S.A., Fischer, A.S., Kindle, J.C., 1998. Atmospheric forcing in the Arabian Sea during 1994 – 1995: observations and comparisons with climatology and models. *Deep-Sea Research Part II* 45, 1961–1999.
- Wessel, P., Smith, W.H.F., 1991. Free software helps map and display data. *EOS* 72, 441, 445–446.